Arcaro, S.; Novaes De Oliveira, A.; Gutierrez-Gonzalez, C.; Salvador Moya, MD.; Borrell Tomás, MA.; Moreno, R. (2017). LZS/Al2O3 nanostructured composites obtained by colloidal processing and spark plasma sintering. Journal of the European Ceramic Society. 37(16):5139-5148. https://doi.org/10.1016/j.jeurceramsoc.2017.03.023

LZS/Al_2O_3 nanostructured composites obtained by colloidal processing and spark plasma sintering

S. Arcaro[1]; A.P.N. Oliveira[1]; C.F. Gutiérrez[2]; M.D. Salvador[3]; A. Borrell[3]; R. Moreno[4]*

[1] Laboratory of Glass-Ceramic Materials (VITROCER), Federal University of Santa Catarina, Florianópolis (SC), Brazil
[2] Centro de Investigación en Nanomateriales y Nanotecnología, CSIC, Principado de Asturias, Spain
[3] Instituto de Tecnología de Materiales, Universitat Politècnica de València, Spain
[4] Institute of Ceramics & Glass, CSIC, Madrid, Spain
* rmoreno@icv.csic.es

ABSTRACT

Li_2O-SiO_2-ZrO_2 (LZS) glass-ceramics have interesting properties as high mechanical strength and hardness and high resistance to abrasion and chemical attack but also high coefficient of thermal expansion (CTE), which can be reduced adding alumina nanoparticles. The conventional melting process is complex and energy consuming, as it requires the melting of the powders to form a glass and a two-step milling process to obtain particle sizes adequate for pressing. This paper describes another route for the preparation of those materials through a colloidal approach from mixtures of SiO_2 and *ZrO_2 nano*powders *and a Li precursor (lithium acetate obtained by reaction of the carbonate with acetic acid). Concentrated suspensions were freeze-dried to obtain homogeneous mixtures of powders that were pressed and sintered by conventional sintering and ~~by~~ spark plasma sintering. The effect of the additions of alumina nanoparticles on suspensions rheology, sintering behavior and properties like constant of thermal expansion were studied.*

Keywords: LZS, suspensions, colloidal processing, spark plasma sintering

1. INTRODUCTION

The increasing technological demand requires the fabrication of materials with enhanced behavior under extreme and variable working conditions so that constant advances in the industry are implemented to overcome the need of new solutions for the most varied applications. It is noticed, in the last 20 years, the emergence of structures with high complexity coming from the combination of the most diverse classes of materials. Moreover, the demand for more efficient materials has stimulated the research of new compounds that have low thermal expansion, since the behavior of materials at different temperatures is crucial in many applications [1, 2].

Materials that have low coefficient of thermal expansion (CTE) are being developed for applications that require rapid temperature variations, such as heat

exchangers [3], refractories for steel casting applications [4], and burner nozzles, among others. In addition, in applications involving bonding of materials, the thermal expansion, requires a very close fit/compatibility, as for example in glass-ceramic/metal systems [5] which are employed as hermetic seals in laser tubes [6], vacuum tubes [7], solid oxide fuel cell sealants [8, 9] and substrates used in electronic micropackaging in low temperature co-fired ceramic (LTCC) technology [10].

The LZS (Li_2O-ZrO_2-SiO_2) is a glass-ceramic system originally obtained by the melting process and the obtained frit is crushed, milled, shaped and finally recrystallized through an adequate thermal treatment. The resulting glass-ceramics contain lithium and zirconium silicates ($Li_2Si_2O_5$ and $ZrSiO_4$) as main crystalline phases and exhibit reasonable good properties such as typical hardness values of 8 ± 0.5 GPa, bending strength of 190 ± 13 MPa and fracture toughness of 3.65 ± 0.20 $MPa \cdot m^{1/2}$. However, there is a limitation regarding to the relatively high coefficient of thermal expansion ~~(CTE)~~ typically ranging from 8.8 – 10 x 10^{-6} $°C^{-1}$ [11-13]. As it has been reported elsewhere the CTE can be reduced by adding alumina to a glass-ceramic composition, by melting a new composition with a lower CTE (4 – 6 x 10^{-6} $°C^{-1}$) [14, 15], or by incorporating particles able to promote a solid state reaction to produce crystalline phases with lower CTE [16-19]. This is the case of the addition of alumina to forms the β-spodumene crystalline phase, which has a very low CTE (0.9 x 10^{-6} $°C^{-1}$). Thus, appropriate amounts of this phase may result in materials with low and controlled CTE suitable for specific applications, as in the case of multilayer materials [17]. Nowadays, the methods of obtaining and modifying properties in vitreous materials are already well known, and the ease of adjusting the composition by the reactivity of particles with smaller sizes has aroused attention. However, the conventional processing requires several steps and ~~in particular is~~ very energy consuming due to the long and energetical milling required to obtain the compacts from the frits. In that sense, it would be interesting to evaluate the possibility of producing similar systems using other routes of synthesis and processing other than by means of fusion processes. The knowledge of the properties of nanostructured materials, for example, is very important as a basis for the development of future technological applications, since significant improvements in properties are expected, greater purity and better homogeneity.

The study of the production and characterization of nanostructured materials has been one of the most attractive topics of fundamental and technological research in the last years, due to the possibilities of improvement of the diverse properties that these materials can have in comparison to materials whose dimensions are in the micrometric scale. Understanding the changes that the properties of the materials present at the nanoscale is essential for the development of new structures and materials for specific applications and with adequate performance. However, the properties of the nanoparticles can contribute positively to the consolidation of the projected materials only if they are processed properly, since the large interparticle forces result in uncommon properties of the powders such as low densities. In this way, the processing step of the powders is of paramount importance. To decrease the amount of agglomerates and to more readily disperse the nanoparticles, colloidal processing is usually used (33). Moreover, a major advantage of using powders with smaller particle sizes is to decrease the sintering temperature, since in this case there is an increase in surface area of the powders. Thus, materials produced from powders with nanometric dimensions are sintered at lower temperatures (200 to 400 ºC) than those used in the sintering of the same materials obtained from powders with particles of micrometric dimensions (34,35).

In this context, the objective of this work is to obtain nanostructured composites of the LZS and LZS/Al_2O_3 systems by reaction sintering of the nanoparticulate oxides using a colloidal approach.

2. Experimental procedure

For the production of a nanoparticulate material with the same composition of a LZS glass-ceramic reported in the literature [20], containing $19.58Li_2O{\cdot}11.10ZrO_2{\cdot}69.32SiO_2$ (mol%), the following raw materials were used: 1) nanosized ZrO_2 powder (40N-0801, Inframat, USA), with an average particle size of $d_{v.50}$ 53 nm and specific surface area of 53.2 $m^2{\cdot}g^{-1}$; 2) a commercial aqueous suspension of amorphous SiO_2 nanoparticles (Levasil 200A, Bayer, Germany) with a solids content of 40 wt%, average particle size of $d_{v.50}$ 15 nm and specific surface area of 205 $m^2{\cdot}g^{-1}$, and 3) Al_2O_3 nanoparticles (Aeroxide® AluC, Evonik-Degussa, Germany), with average particle size $d_{v.50}$ 13 nm and specific surface area of 100 $m^2{\cdot}g^{-1}$. In addition, as precursors for the preparation of lithium acetate, used as a

source of lithium, lithium carbonate (Synth, Brazil) and acetic acid glacial (Quimex, Peru) were used.

Initially, a solution containing deionized water, lithium carbonate and acetic acid glacial was prepared. To achieve the solubility of the lithium carbonate required to obtain the chemical composition of LZS, it was necessary to prepare a solution of 5 $mol \cdot l^{-1}$ of acetic acid glacial. The lithium carbonate was then hydrolyzed in the acetic acid glacial solution to favor the solubility of lithium ions and to eliminate the carbonate in the form of carbon dioxide, according to reaction (1):

$$Li_2CO_3 + 2CH_3COOH \rightarrow 2\ CH_3COO^- + Li^+ + CO_2\uparrow + H_2O \qquad \text{(Reaction 1)}$$

The lithium ions remain free in the solution and the resulting hydrolyzed salt (acetate) generates a strong base, releasing OH^- according to reaction (2):

$$2CH_3COO^- + H_2O \rightarrow 2CH_3COOH + OH^- \qquad \text{(Reaction 2)}$$

The solution was maintained under constant agitation in a mechanical agitator (200 RW digital, IKA, Germany) at room temperature (T = 25 °C) for 1 h to complete solubilisation of the components. The pH of the resulting solution was checked and maintained at 11. Subsequently, ZrO_2 nanopowder was added slowly, and finally the aqueous suspension containing the SiO_2 nanoparticles was incorporated. The resulting suspension of precursor nanoparticles of the LZS system was maintained under mechanical stirring for 1 h and subjected to ultrasonic dispersion (UP 400S, dr. Hielscher Ultrasonics GmbH, Germany, with a power of 400 W). For the preparation of the LZS/Al_2O_3 mixtures, the same procedure was used and alumina nanoparticles were slowly added in volumetric concentrations of 1, 2.5 and 5% in a latter step.

The colloidal stability was studied by measuring the variation of zeta potential of the raw materials as a function of pH using laser Doppler velocimetry (Zetasizer NanoZS, Malvern, UK). For this purpose, suspensions with a solid concentration of 0.1 $g \cdot l^{-1}$ were prepared in a 10^{-3} M KCl aqueous solution by ultrasonic mixing for 1 min. The pH control was done using 10^{-1} M HCl and KOH solutions. The rheological characterization of the suspension of the precursor mixture of the LZS system was carried out using a rheometer RS50 (Thermo Haake, Germany) with a double-

cone/plate sensor configuration (DC60/2, Thermo Haake, Germany) that requires a sample volume of 5-10 ml and the testing temperature was maintained at 25 °C. The flow behavior was measured by controlled rate (CR) tests employing a measuring program in three stages: first a linear increase of shear rate from 0 to 1000 s^{-1} in 3 min; a plateau at the maximum shear rate (1000 s^{-1}) for 30 s; and a decrease to zero shear rate in 3 min.

Once optimized the rheological behavior selected suspensions were placed in a volumetric flask, which was coupled to a rotary evaporator (120 rpm, RV 10 basic, IKA, Germany), and frozen in a liquid nitrogen bath. Once frozen the suspensions were freeze-dried (Cryodos 50, Telstar, Spain) to remove the ice by sublimation, the operating conditions being a vacuum of 5 Pa and -50 °C. The material was kept in the freeze dryer for 24 h. The sublimation of the ice gave rise to the formation of agglomerates of spherical morphology. For de-agglomeration a planetary mill (250 rpm, MW 100, Retsch, Germany) was used for 5 min.

The chemical analysis of the precursor of the LZS system obtained was performed by the X-ray fluorescence technique (FRX, PW 2400, Philips, The Netherlands). The lithium fraction was determined by atomic absorption spectrometry (969, Unican, UK).

Samples of the LZS and the LZS + Al_2O_3 compositions were subjected to differential thermal analysis (DTA) and thermogravimetric (TG, SDT Q600, TA Instruments, USA) tests. From these thermal analyses, it was possible to determine the calcination temperatures for the removal of the organic material, crystallization, melting, and the physico-chemical reactions that occur with the materials when subjected to thermal treatments. The analyses were performed in an oxidizing atmosphere (air) at a heating rate of 10 °C·min^{-1} in a temperature range between 25 and 1300 °C, using a platinum crucible and an empty reference material. Dilatometric analyses were performed using an optical dilatometer (ODHT, Expert System Solution, Misura, Italy) such that the thermal shrinkage curves were obtained. The samples were heated until melting, with a heating rate of 10 °C/min, in an oxidizing (air) atmosphere.

Thus, samples of these compositions were uniaxially pressed in a cylindrical steel die by means of a hydraulic press (ST Bovenau P10, Brazil) at 100 MPa. The obtained samples were dried at 110 °C for 2 h. In a subsequent step, the dried samples were fired at 900, 950, 1000, 1050, and 1100 ºC during different times (30,

120 min), and different heating rates (1, 5, and 10 °C·min^{-1}) and cooled to room temperature. Furthermore, a non-conventional firing process was also used. For this, powders of the same compositions as those pressed and sintered were subjected to a fast firing process using the spark plasma sintering technique (SPS). Initially, powders were introduced into graphite mold and pressed uniaxially at 10 MPa. Then the compacts obtained were introduced into the SPS (HP D-25, FCT System Gmbh, Germany) and heated by electric current at a rate of 100 ºC·min^{-1} under a pressure of 80 MPa, to the temperature of 850 °C with a pulse duration of 1 min.

The true densities (ρ_t) of powdered samples were determined by using a helium pycnometer (AccuPyc 1340, Micromeritics, USA). The apparent densities (ρ_a) of fired samples were determined by relating their geometrical measurements, obtained using a caliper (Mitutoyo, Japan, accuracy ± 0.01 mm), and their masses (Shimadzu AX200, Japan, at 0.001 g). The relative densities (ρ_r) were determined relating the apparent densities and the true densities of the samples according to Eq. 1.

$$\rho_r = (\rho_a / \rho_t) \times 100 \qquad \text{(Eq. 1)}$$

The crystalline phases of the LZS system with and without additions of Al_2O_3 nanoparticles in the samples subjected to heat treatments were identified by X-ray diffraction analysis (Philips, model X'Pert, The Netherlands) using the CuKa radiation (1.5418 Å) at 40 kV and 30 mA. Samples were rotated to minimize the effect of preferential orientation and analyzed in powder form with particle size smaller than 45 µm, using a step size of 0.02, dwell time of 2 s per step and 2θ between 5 and 80 º. ICSD and JCPDS data banks were used for identification of the resulting crystalline phases. The crystallite sizes for nanoparticulate materials (D) were calculated using Scherrer equation (Eq. 2):

$$D = \frac{k\lambda}{\beta cos\theta} \qquad \text{(Eq. 2)}$$

where k is a constant whose value is 0.9999, λ the wavelength of the incident radiation used, β the width of the half height in radians of the most intense peak and θ the angle of Bragg in degrees. The quantitative analysis of the crystalline phases was performed by the Rietveld method [21-23]. The refinement of the X-ray patterns

as well as the simulation and quantification of the crystalline phases were performed by the X'Pert HighScore Plus® software (Philips, The Netherlands).

In order to evaluate the morphological characteristics of the precursor of the nanoparticulate LZS system, a transmission electron microscope (JEM 2011, JEOL, Japan) was used, after the freeze-drying and calcination process, with a 100 kV intensity. The samples were dispersed in acetone for 10 min of ultrasound. The microstructure of the fired samples was observed on fracture surfaces using a field emission gun scanning electron microscope (FE-SEM, S-4800 type I, Hitachi, Japan).

The coefficient of thermal expansion (CTE) of the composites was determined using a contact dilatometer (Netzsch Gerätebau model 402 EP, Germany) at a heating rate of 5 °C·min^{-1} in the temperature range between 25 and 500 °C.

The thermal conductivity of the composites was determined using a Tci Thermal Conductivity analyzer (C-THERM TECHNOLOGIES) on sintered discs with 30 mm in diameter and 5 mm in thickness.

Mechanical properties of the composites were evaluated via nanoindentation techniques. Hardness (H) and Young's modulus (E) were analysed by a nanoindenter G-200 of Agilent Technol. (Inc., Santa Clara, CA) under a 2000 nm constant indentation depth program. A Berkovich tip was used after calibration of the function area in fused silica. Stiffness was recorded in depth by Continuous Stiffness Measurement (CSM). The oscillation amplitude was programmed to 2 nm with a frequency of 45 Hz.

3. RESULTS AND DISCUSSION

Figure 1 shows the variation of zeta potential of zirconia and silica nanoparticles with pH. It can be seen that the value found for the iep for ZrO_2 was lower than pH 2. This is an unexpectedly low IEP for zirconia that suggests that its surface is being modified by the presence of some additives used during its manufacture. For pH values greater than 2, it was observed that the zeta potential value increases continuously until pH 7, remaining constant for increasing pH values. For these alkaline pH values, the zeta potential is as high as -50.0 mV, indicating that under these pH conditions it is possible to prepare stable suspensions with the commercial ZrO_2 nanoparticles. For the SiO_2 nanoparticles, it can be seen that the iep could not be measured but it is close to pH 1. In addition, the zeta potential increases

continuously with increasing pH up to the measured value of pH 9, with zeta potential greater than -30 mV, indicating a stability of commercial SiO_2 nanoparticles at this pH. As can be seen, the SiO_2 particles are negatively charged at any pH, which suggests the presence of adsorbed molecules on the silica surface needed to keep the particles dispersed in the commercial colloidal suspension used [24]. For Al_2O_3 the isoelectric point occurs at pH 10. The improved dispersion and stabilization occurs at a basic pH, i.e., above 11. Therefore, for stabilizing blends of Al_2O_3 and LZS glass, strongly alkaline pH must be used.

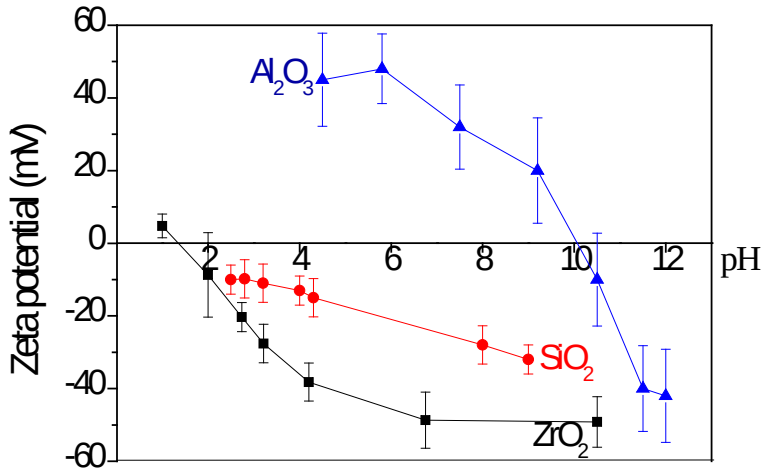

Figure 1: Variation of zeta potential of zirconia and silica nanoparticles with pH.

The high values of zeta potential indicate high stability of the nanoparticles in suspension at alkaline pHs, as the similarly charged particles repel each other and this force overcomes the natural tendency to aggregation induced by the London-van der Waals forces [25]. Accordingly, the suspensions prepared by mixing these nanoparticles of ZrO_2, SiO_2 and Al_2O_3 display a good stabilization in which the formation of agglomerates by heterocoagulation is prevented. When the ZrO_2, SiO_2 and Al_2O_3 nanoparticles were added to the lithium acetate solution, there was a contribution of the OH^- ions to increase the pH of the final suspension. In fact, the pH measured for the resulting suspension was 11, thus facilitating, at a later stage, the effectiveness of the synthesis of the precursors of the LZS system by the dispersion of the nanoparticles. After the stabilization of the reaction and the addition of the zirconia nanoparticles first and the colloidal silica suspension, later, the stability of the

suspensions was evaluated by measuring their rheological behavior, as can be visualized in the flow curves obtained as a function of sonication time shown in Figure 2.

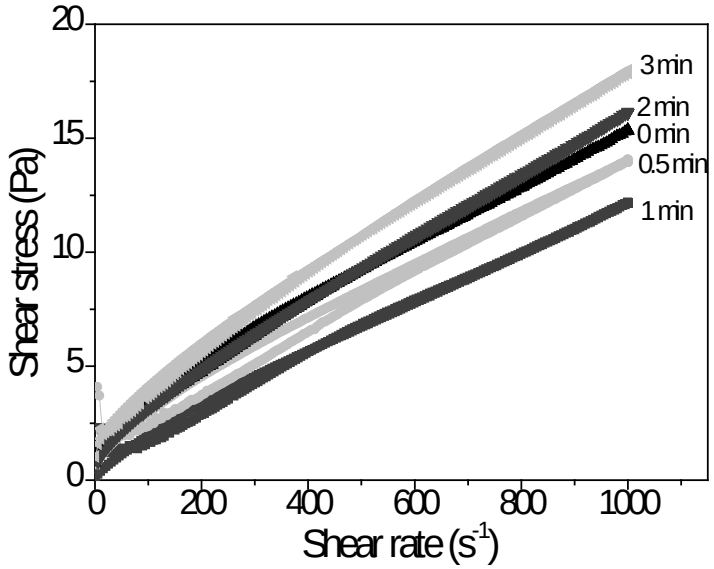

Figure 2: Flow curves for the suspension of the precursors of the LZS system obtained by dispersion using different sonication times.

It is possible to observe that the suspensions obtained for the precursors of the system LZS, have low viscosity, without hysteresis, or other signs of agglomeration. This can be explained considering the low solids content of those suspensions (~18 vol.%). The dispersion with ultrasounds for 1 min was effective to undo weak agglomerates between the particles, but 2 min of ultrasounds produces a slight re-agglomeration of the particles.

Figure 3 shows the curves of differential thermal and thermogravimetric analysis of the powders obtained by freeze-drying of the suspensions. It is possible to observe by thermogravimetry (TG) that there is a total mass loss of approximately 25%. The first step of this mass loss corresponds to 4% and occurs in the temperature range of 30 - 100 °C, and refers to the elimination of moisture present in the material. In the temperature range of 100 - 300 °C it is possible to observe a mass loss of 4%, which is accompanied by three exothermic events ((a), (b) and (c)), and may be related, in addition to dehydration of the powder the combustion of acetic acid (146). At temperatures between 300 and 550 °C, the slope of the TG curve changes, denoting a more vigorous mass loss. Following this loss of mass of 17%, we observe an

intense exothermic peak with a maximum of 405 °C, which corresponds mainly to the elimination of the organic additives molecules used in the preparation and stabilization of the colloidal silica suspension [24]. Subsequently, at 580 ºC, an exothermic peak can be observed, which may be related to a crystallization event, probably of phases containing lithium silicates. Based on these results, it was possible to define the calcination temperature of the precursor powders of the LZS system at 600 °C, since from this temperature there are no more organic materials that could hinder the subsequent processing steps. The selected heating rate was relatively slow (0.5 °C·min^{-1}), and the residence time, at the selected temperature, set at 4 h, to ensure that the 25% of organic materials present could be eliminated. In the compositions with additions of other oxides in the stoichiometric mixture of lithium disilicate, the results of the literature indicate that the Li_2SiO_3 decomposes completely above 820 °C, where lithium disilicate predominates ($Li_2Si_2O_5$), which justifies the exothermic peak observed [26] (f). The endothermic event observed at approximately 955 °C (g) can be attributed to the melting of the crystalline phases containing lithium ($Li_2Si_2O_5$ - Tm = 1033 °C) [27].

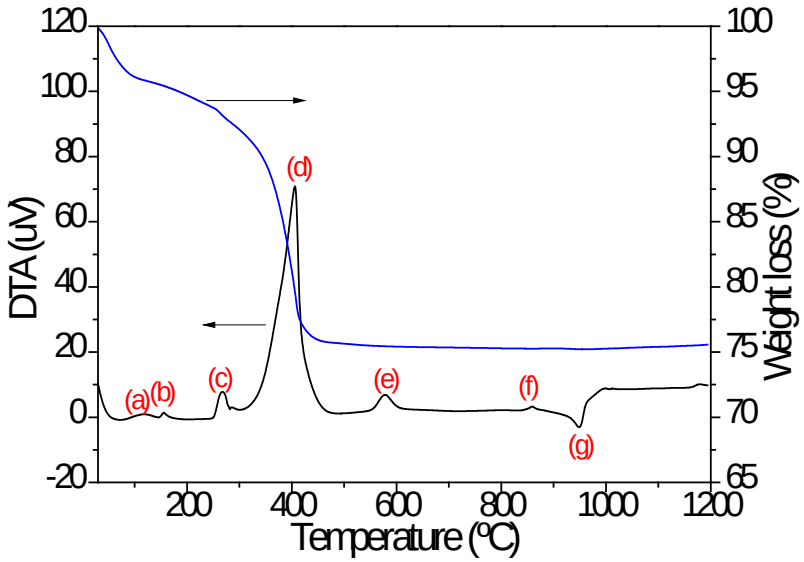

Figure 3: Differential Thermal Analysis (DTA) and thermogravimetry (TG) curves obtained for the LZS freeze-dried powder.

Table 1 presents the results of the chemical analysis of the precursors of the LZS system. As can be seen a small difference for lithium oxide with respect to the theoretical concentration can be observed. This fact may have occurred because

lithium is free in the aqueous medium and can be physically dragged during sublimation of ice in the freeze-drying step. In the case of sodium oxide, contamination may be associated with stabilization of commercial nanoparticles, since SiO_2 nanoparticles, for example, are stabilized with additives containing Na_2O [24]. Even so, these oxides, in small amounts, apparently did not affect the expected performance of the LZS system obtained by this route, since the purity of the obtained materials is superior to 99%.

Table 1: Chemical composition of the precursors of the nanoparticulate composite LZS.

Oxides	**Theoretical concentration [20]**	**Determined concentration**
Al_2O_3	---	---
CaO	---	---
Fe_2O_3	---	---
Li_2O	9.56	9.16
Na_2O	---	0.51
SiO_2	68.1	67.85
TiO_2	---	---
ZrO_2	22.4	22.48

Figure 4 shows the X-ray diffraction pattern of the precursor powder of the nanoparticulate LZS system just after freeze drying (i) and after calcination at 600 °C (ii) and a microphotography obtained by transmission electron microscopy showing the morphological appearance of the powders of the precursor LZS nanoparticles. It was possible to visualize the primary particles by TEM and to evaluate the average diameters of the nanoparticulate LZS precursor powders with the aid of SizeMeter Software. It can be seen that the powder of the nanoparticulate precursor LZS is, in fact, formed by primary particles of about 25 nm.

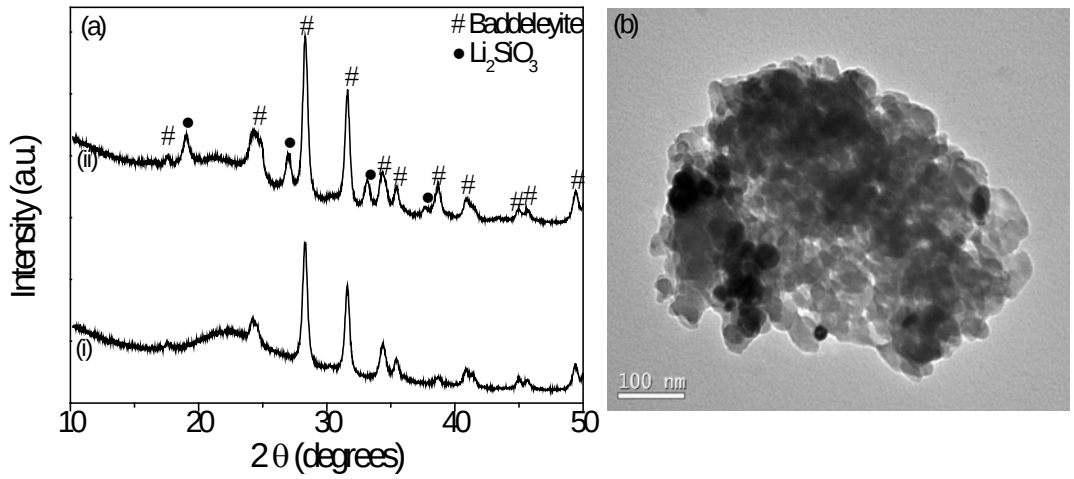

Figure 4: (a) X-ray diffraction pattern of the precursor powder of the nanoparticulate LZS system just after freeze-drying (i) and after calcination at 600 °C (ii) and (b) TEM microphotograph showing the morphological appearance of nanoparticulate LZS precursor powders.

The XRD pattern shown in Figure 4 exhibits a small increase in the reflection occurring at around 23 °, amorphous phase characteristic of the amorphous silica used. In addition, characteristic peaks of the baddeleyite phase (crystalline phase of the monoclinic zirconia JCPDS 36-0420) can be observed in both cases. With calcination at 600 °C (b), it is also possible to observe the formation of the lithium metasilicate phase (Li_2SiO_3, JCPDS 29-0829), as predicted from the DTA curve. An enlargement of crystalline X-ray diffraction peaks is observed, which is an indication that the material is composed of very small crystals (with nanometric scale sizes) [28]. For the crystalline materials, the size of the primary particles can be estimated by using the Scherrer equation, according to which the value is by 26 nm and does not change at the selected calcination temperature. It can be seen that the crystallite sizes are very similar to those obtained from the particle size distributions and the TEM images.

Figure 5 shows the linear shrinkage curve of the precursor powders of the nanoparticulate, calcined LZS system where it is possible to observe that the densification starts at approximately 800 °C and continues up to 1150 °C, where the slope of the curve changes because the melting of the crystalline phases begins. The high reactivity of the nanoparticles, process combined with the high concentration of the lithium alkaline ion, promote the densification and subsequent shrinkage of the

composites. In addition, it may be noted that the addition of alumina causes a greater shrinkage of the material. This fact may be related to the reaction of alumina nanoparticles with lithium at lower temperatures, forming a low viscosity liquid phase, which enhances sintering.

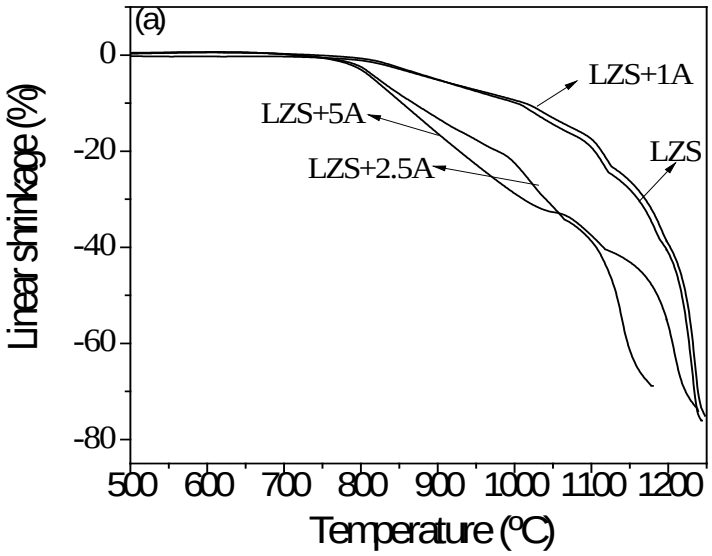

Figure 5. Linear shrinkage curves for powders of the precursor of the nanoparticulate LZS system and LZS + Al_2O_3 compositions after calcination at 600 °C.

For the study of conventional sintering of the composites, different heating schedules were tested maintaining the firing temperature at 1050 ºC and changing the heating rate (1, 5, and 10 °C·min^{-1}), and the dwell time (30 and 120 min). The relative density obtained for the LZS composites subjected to the different thermal treatments is shown in Table 2. It can be clearly seen that lower heating rates promote a higher densification of the nanostructured LZS composite. For a heating rate of 10 °C·min^{-1}, a relative density of approximately 75 % was achieved at 1050 °C - 30 min, whereas for the lowest heating rate, i.e. 1 ºC·min^{-1}, a relative density of 84.5 % was reached. Moreover, a longer dwell time of 120 min gave a better relative density (~87%) than 30 min (~ 85%). Possibly, longer residence times, associated with lower heating rates are more efficient to densify these materials when using conventional firing techniques, leading to longer times for the nanoparticles to sinter and rearrange, which results in materials with a lower porosity. After the determination of the heating rate (1 °C·min^{-1}) and the dwell time (120 min), all composites (LZS, LZS + 1A, LZS + 2.5A, LZS + 5A) were fired at different

temperatures (900, 950, 1000, 1050, 1100 °C). It is noteworthy that the composites LZS + 2.5A and LZS + 5A, fired at 1050 and 1100 ºC suffered a significant shrinkage and lose their cylindrical shape, so that it is no longer possible to continue the characterization of these materials. This fact can be explained by the liquid phase formed by the melting of lithium crystalline phases at temperatures above 1000 ºC, as already observed in the thermal analysis graphs (Figure 5).

Table 2. Relative density values for nanostructured composites, fired at 1050 °C for 30 min, as a function of the heating rate and fired at 1050 °C, at a heating rate of 1 °C·min^{-1} as a function of the dwell time.

Heating rate (ºC/min)	Dwell time (min)	Relative density (%)
1	30	84.5 ± 0.5
1	120	86.5 ± 0.5
5	30	80.3 ± 0.5
10	30	75.2 ± 0.3

In Table 3 it can be seen that the relative density of the nanostructured composites fired by conventional sintering varies from about 55 to 91% in the temperature range of 900-1100 °C. The relative density of the nanostructured composites is very low at even 950 ºC and only when the firing temperature increases to 1000 °C densification takes place, although the densities maintain still low (85-91% of theoretical). At temperatures above 1000 °C, for the composites LZS and LZS + 1A, there were no significant variations in the relative density and for higher alumina contents the samples deform excessively.

Table 3. Effect of the firing temperature for samples fired at a rate of 1 °C·min^{-1} for 120 min on the relative density, ρrel (%), calculated from powder compacts of the nanostructured LZS composite and compositions LZS + Al_2O_3 and relative density values calculated from powder and powder samples of the nanostructured LZS and LZS + Al_2O_3 compositions by SPS at a temperature of 850 °C for 1 min (100 °C·min^{-1}, 80 MPa).

	Conventional sintering					**SPS**
Composites	***900 ºC***	***950 ºC***	***1000 ºC***	***1050 ºC***	***1100 ºC***	***850 ºC***
LZS	54±1.0	58±0.8	85±0.3	86±0.3	86±0.6	92±0.5
LZS+1A	55±0.8	60±0.5	86±0.2	86±0.8	87±0.5	93±0.5

LZS+2.5A	67±0.5	70±0.3	91±0.5	-	-	95±0.5
LZS+5A	54±0.5	58±0.5	85±0.3	-	-	96±0.5

Based on the observed relative density and linear shrinkage results, and the evolution of the crystalline phases observed for the LZS and the LZS + Al_2O_3 composites, the firing schedule selected for further characterization was 1000 °C-120 min at a heating rate of 1 °C·min^{-1}. However, in view of the difficulty in achieving relative densities above 90% by conventional sintering, alternative firing techniques are necessary in order to activate densification mechanisms at temperatures below any possible melting can occur. The non-conventional SPS technique uses pulses of electric current for rapid sample heating, coupled with the simultaneous application of pressure, promoting a better packing of the particles and aiding in the removal of pores. The determination of the parameters involved in the firing was performed through preliminary tests that demonstrated that a heating rate of 100 ºC·min^{-1}, a pressure of 80 MPa and a dwell time of 1 min are sufficient for the sintering of the materials. Based on the optical dilatometry curves, the final firing temperature of 850 °C was selected. It is worth mentioning that temperatures above 850 ºC caused the composites to melt, which is detrimental to the materials and to the SPS (furnace) system. Temperatures below 850 °C are not sufficient to densify the material by SPS, since, according to the optical dilatometry curves, at 800 °C no densification takes place yet. In Table 3 the relative density values of the nanostructured LZS and LZS + Al_2O_3 composites containing 1, 2.5 and 5% Al_2O_3 sintered by SPS at a temperature of 850 °C for 1 min are also shown.

In fact, the sintering through SPS allowed reaching high densification. The relative density values increase from 92 to 96% with increasing amount of Al_2O_3. It can also be observed that the relative densities were higher than those achieved by conventional sintering. In addition, SPS temperatures in were approximately 150 ºC below those used in conventional sintering, in addition to a shorter residence time.

Figure 6 shows the microstructure obtained by SEM of the fracture surface of samples of nanostructured LZS system and LZS + Al_2O_3 composites obtained by conventional sintering at 1000 °C for 120 min. It can be seen, in general, that the addition of alumina improved the densification, in terms of reducing the porosity of the obtained composites, as expected. For the compositions LZS (Figure (a, f)), and LZS + 1A (b), the microphotographs show that although the sintering temperature

used was sufficient to densify the compacts to acceptable levels, the high degree of agglomeration causes a differential shrinkage between the agglomerates and creates voids in the structure (porosity between clusters), as can be observed even in microphotographs taken with larger magnification (Figure 6(f)). For the composites LZS + 2.5A and LZS + 5A, a greater densification and more closed pores are appreciated.

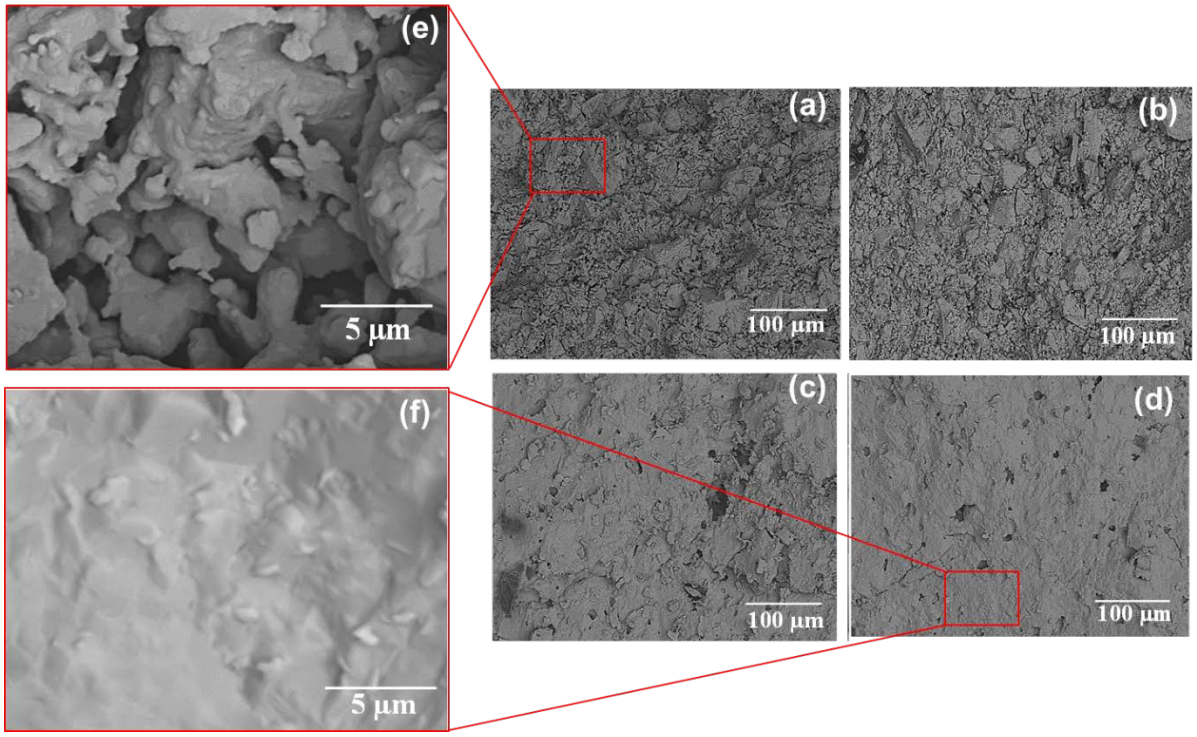

Figure 6: SEM Microphotographs of the fracture surface of the nanostructured LZS (a, f) system, and composites LZS + 1A (b), LZS + 2,5A (c), LZS + 5A (d, g) obtained by conventional sintering at 1000 º C - 120 min.

Figure 7 shows the SEM microstructure of the fracture surface of the nanostructured LZS (Figure 7(a)(e)) and composites LZS + 1A (Figure 7(b)), LZS + 2.5A (Figure 7 (c)), LZS + 5A (Figure 7 (d)(f) fired by SPS at 850 °C for 1 min. It is verified that in fact it was possible to obtain samples with densities close to the theoretical. The microstructure obtained is relatively dense and more homogeneous than that of composites obtained by conventional sintering. It can be observed that similarly to conventional sintering, the addition of alumina caused an enhancement in the densification, because in the composites LZS and LZS + 1A, it is possible to visualize a larger porosity, even with closed pores. For the composites LZS + 2.5 and LZS + 5A a reduction of the pore size is also verified. Another interesting result that

can be observed is the microstructural homogeneity, and the little grain growth, provided by the SPS sintering method, since it is possible to observe the resulting nanostructure.

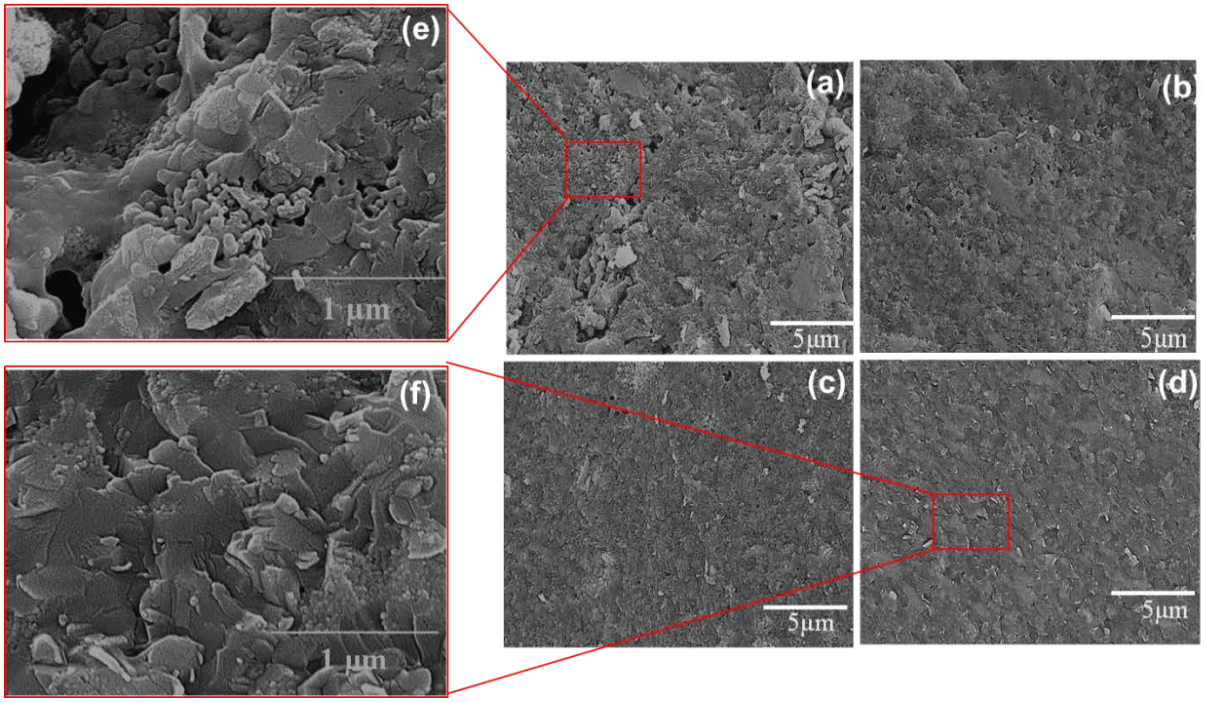

Figure 7. SEM microstructure of the fracture surface of the composites LZS (a, e) LZS + 1A, LZS + 2,5A, LZS + 5A, fired by SPS at 850 ºC for 1 min.

Figure 8 shows the X-ray diffraction patterns, and Table 4 the relative percentages of the crystalline phases found after the Rietveld refinement of the nanostructured LZS system and the composites LZS + 1A, LZS + 2.5A and LZS + 5A fired at 1000 ºC. for 120 min by conventional sintering (a) and fired at 850 °C for 1 min by SPS (b).

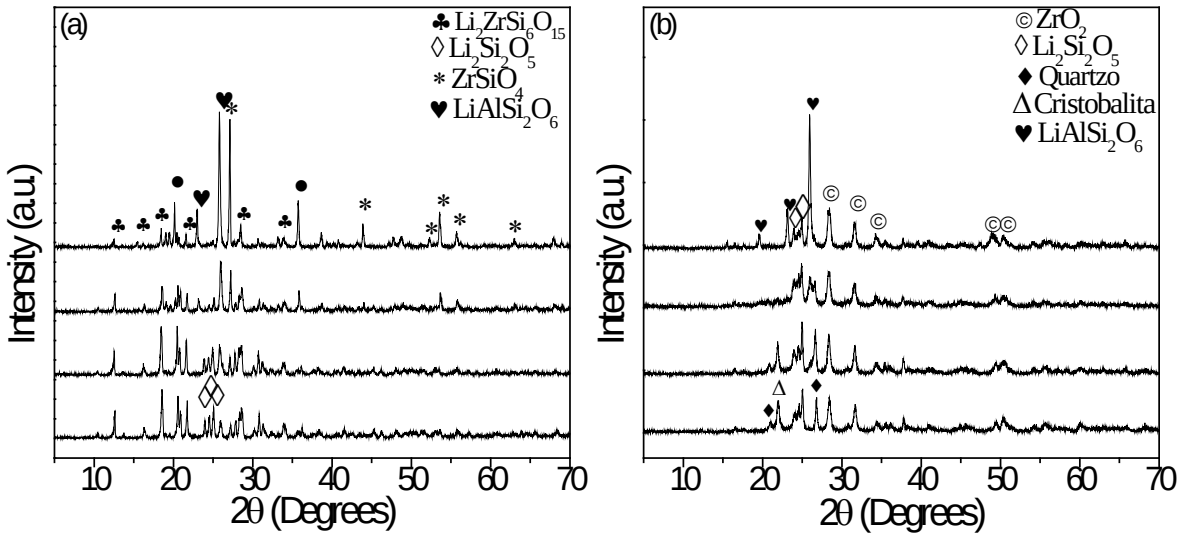

Figure 8. X-ray diffraction patterns, of the nanostructured LZS system and the composites LZS + 1A, LZS + 2.5A and LZS + 5A fired at 1000 ºC for 120 min by conventional sintering (a) and fired at 850 °C for 1 min by SPS (b).

Table 4. Relative crystalline fraction of composite samples of the nanostructured LZS system and composites LZS + 1A, LZS + 2.5A and LZS + 5A fired at 1000 ºC for 120 min by conventional sintering and fired at 850 ºC for 1 min by SPS sintering.

Crystalline phase	**Crystalline fraction (wt%)***							
	Conventional sintering				**SPS sintering**			
	LZS	**LZS+1A**	**LZS+2.5A**	**LZS+5A**	**LZS**	**LZS+1A**	**LZS+2.5A**	**LZS+5A**
$ZrSiO_4$	2.3	3.4	9.7	20.4	-	-	-	-
$Li_2Si_2O_5$	20.8	18.7	2.4	1.9	44.3	43.2	31.7	18.9
$Li_2ZrSi_6O_{15}$	74.3	67.6	47.8	15.0	-	-	-	-
$LiAlSi_2O_6$	-	7.7	29.0	51.2	-	8.2	26.5	58.1
Li_2SiO_3	2.6	2.5	11.0	11.6	-	-	-	-
m-ZrO_2	-	-	-	-	18.5	18,5	18.5	18.5
Quartz	-	-	-	-	15.7	14.1	13.2	4.6
Cristobalite	-	-	-	-	21.6	16.0	-	-

$ZrSiO_4$, zirconium silicate, ICSD 69644; $Li_2Si_2O_5$, lithium disilicate (ICSD 15414); $Li_2ZrSi_6O_{15}$ (ICSD 100631)); β-Spodumene $LiAlSi_2O_6$ (ICSD 14235); Li_2SiO_3, lithium metasilicate (ICSD 28192); m-ZrO_2, monoclinic zirconia (ICSD 41010); Quartz, SiO_2 (ICSD 16331); Cristobalite, SiO_2 (ICSD 47440).

The phase analysis reveals that the LZS material subjected to the conventional firing process has 2.3% $ZrSiO_4$, 20.8% $Li_2Si_2O_5$, 2.6% Li_2SiO_3 and 74.3% $Li_2ZrSi_6O_{15}$ phase. This last is probably the most stable phase for this system, and has already been found in Li_2O-ZrO_2-SiO_2-systems with other molar compositions obtained either

by reaction in the solid state or by sol-gel synthesis [29-31]. When Al_2O_3 is added, there is a gradual decrease of the crystalline phase $Li_2ZrSi_6O_{15}$ and also of the $Li_2Si_2O_5$, besides the formation of $LiAlSi_2O_6$ with a considerable increase of the relative amounts of the phases $ZrSiO_4$ and Li_2SiO_3. This phenomenon probably happens because Al_2O_3 has high affinity with lithium, and they react to form $LiAlSi_2O_6$. For this reaction to occur, the phase $Li_2ZrSi_6O_{15}$ is consumed, also forming $ZrSiO_4$. Since there is no SiO_2 available system, dissociation occurs of $Li_2Si_2O_5$ in Li_2SiO_3, according to reaction 3.

$Li_2Si_2O_5 \rightarrow Li_2SiO_3 + SiO_2$ (Reaction 3)

It is observed that the higher the addition of Al_2O_3 in the system, the greater the amount of $LiAlSi_2O_6$ formed, ranging from 7.7% (LZS+1A) to 51.2% (LZS+5A).

It can be seen that the composites sintered by SPS showed strong differences with the counterparts obtained by conventional sintering, related to the type and relative amounts of the crystalline phases formed. It is first noticed that there was no formation of zirconium silicate. Note that the crystalline phases formed were ZrO_2 (18.5% for all composites), $Li_2Si_2O_5$ and quartz. As already occurred for the other systems, the addition of alumina caused the $LiAlSi_2O_6$ phase to appear. As expected, this crystalline phase gradually increases as there are higher amounts of Al_2O_3 in the composites (LZS+1A = 8.2%, LZS+2.5A = 26.5%, LZS+5A = 58.1%). However, in this case, there was no formation of Li_2SiO_3, since there was SiO_2 (quartz and cristobalite) available in the system for the reaction to occur in a balanced way. In fact, it was found that there was a decrease in the silica content with the addition of alumina.

Figure 10 compares the CTE of the nanostructured LZS system and the composites LZS + 1A, LZS + 2.5A and LZS + 5A fired at 1000 ºC for 120 min by conventional sintering and fired at 850 ºC for 1 min by SPS. According to the plot the CTE decreases with the amount of Al_2O_3 added for both series of materials. For composites fired by conventional firing process, the CTE decreased from 5.8 for the nanostructured LZS composite to 2.2 x 10^{-6} $°C^{-1}$ for the LZS + 5A composite. In the case of composites fired by SPS, the CTE decreases from 11.8 for the nanostructured LZS composite to 4.7 x 10^{-6} $°C^{-1}$ for the composite LZS + 5A. This significant decrease in CTE with the increasing amount of Al_2O_3 added is related to

the formation of the β-spodumene phase (which has a low CTE, 0.9 x 10^{-6} °C^{-1}) as indicated in the structural analysis (Figure 8 and Table 4). It is worth noting that the differences observed for the CTE of the composites sintered by conventional sintering or SPS are probably due to the difference of the crystalline phases present in these materials. The composites obtained by SPS, have higher CTE when compared to the same composites subjected to the conventional firing process. This fact is probably related to the presence of the crystalline phase ZrO_2, which has a high CTE value, 13 x 10^{-6} ºC^{-1} [32].

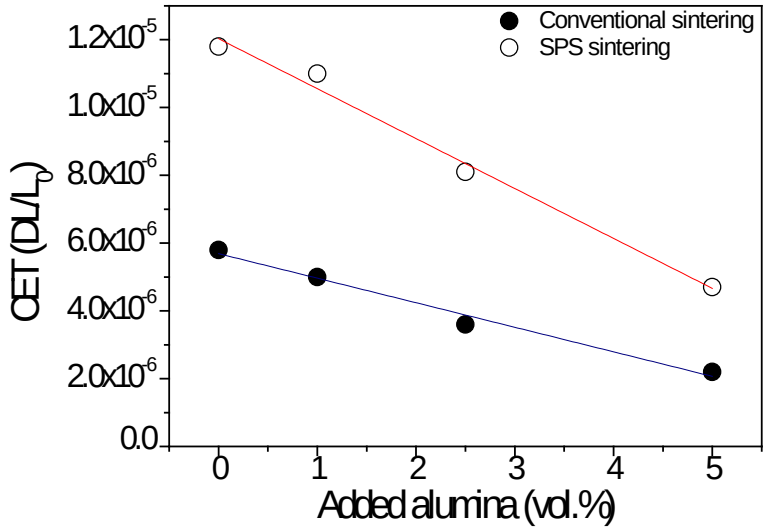

Figure 9. CTE of the nanostructured LZS system and composites LZS + 1A, LZS + 2.5A and LZS + 5A fired at 1000 ºC for 120 min by conventional sintering and fired at 850 ºC for 1 min by SPS sintering.

Table 5 shows the thermal conductivity of the composite of the nanostructured LZS system and the composites fired by conventional sintering and by SPS. It can be observed that the thermal conductivity in both cases increases with the amount of alumina added, varying between 1.10 and 3.60 $W \cdot m^{-1}K^{-1}$. Such increase may be related to the negative influence of the closed porosity on the thermal conductivity. Closed pores can be considered a phase of low thermal conductivity dispersed in the structure, because they are full of air and the air is poor conductor of heat. Despite this increase, the thermal conductivity of these materials is so low that it does not compromise its use as a thermal insulation.

Table 5. Thermal conductivity of the composite of the nanostructured LZS system and the composites LZS + 1A, LZS + 2.5A and LZS + 5A fired at 1000 ºC for 120 min by conventional sintering and fired at 850 ºC for 1 min by SPS sintering.

Added alumina (vol.%)	Conventional sintering	SPS sintering
0	1.10±0.10	3.00± 0.10
1	1.90±0.10	3.10± 0.05
2.5	2.30±0.05	3.60± 0.05
5	2.55±0.05	3.35± 0.05

In Figure 10(a) it can be observed that the Vickers hardness of the nanostructured composites sintered by the conventional process of LZS with up to 1% alumina was very low, not exceeding 1 GPa, a fact that can be explained by the high porosity of these composites that cannot stand during the tests. The increase of Al_2O_3 concentration to 2.5 and 5% (LZS+2.5A~~n~~ and LZS+5A~~n~~) decreased porosity, and consequently increased Vickers microhardness values to approximately 5 GPa. As for the composites sintered by SPS, the Vickers hardness values were high. Although the relative density values were similar for all composites, the composite with 5A~~n~~ achieved hardness values twice those obtained from measurements performed on nanoparticulate LZS. In this case, what be influencing are, the crystalline phases formed, and the microstructure more homogeneous formed with the addition of Al_2O_3.

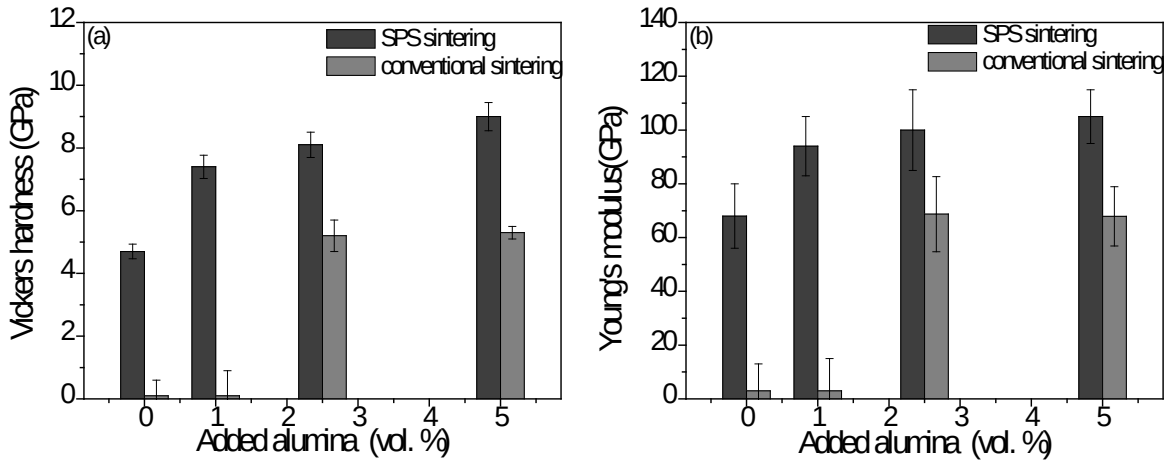

Figure 10. Vickers hardness (a) and Young's modulus (b) values of the composite of the nanostructured LZS system and the composites LZS + 1A, LZS + 2.5A and LZS

+ 5A fired at 1000 ºC for 120 min by conventional sintering and fired at 850 ºC for 1 min by SPS sintering.

Similarly, the Young's modulus (Figure 10(b)) for the materials without and with 1% alumina obtained by conventional sintering was very low, not exceeding 20 GPa, which can be explained again by the high porosity of these composites. Increasing the addition of Al_2O_3 to 2.5 and 5% the porosity decreased, and consequently the Young's modulus values increased to approximately 70 GPa. For the composites sintered by SPS, Young's modulus behaves like the microhardness, that is, the addition of the alumina caused an increase of the Young's modulus ranging from 78 to 105 GPa. This fact may be related to a better structural homogeneity of the material and a reduction of the porosity when the alumina is added.

4 CONCLUSIONS

It has been demonstrated the feasibility of the synthesis of the precursors oxides of the system LZS with a composition $19.58Li_2O{\cdot}11.10ZrO_2{\cdot}69.32SiO_2$ by the dispersion of nanoparticles of ZrO_2, SiO_2 and a lithium precursor obtained from the reaction of lithium carbonate and acetic acid. Concentrated suspensions were dispersed in water at pH 11, subsequently frozen in liquid nitrogen and freeze-dried to obtain nanopowders with primary particles of ~25 nm in diameter. The resulting powders were sintered, on one hand, conventionally at 1000 °C leading to the formation of the crystalline phases $Li_2ZrSi_6O_{15}$, lithium disilicate, and zirconium silicate, achieving maximum relative densities of 90%. On the other hand, the powders were sintered via SPS at 850 °C, forming zirconium oxide, cristobalite, quartz, and lithium disilicate and relative densities between 92 and 96%. The composites containing LZS and between 1 and 5% Al_2O_3, fired at 1000 °C-120 min, resulted in materials hardness of up to 5 GPa and Young's modulus between 20 and 70 GPa, being always the highest values for the LZS+5A nanostructured composite. The thermal conductivity varied by about 1.1 and 2.55 $W{\cdot}m^{-1}K^{-1}$ and the CTE also varied within a relatively large range, i.e. between 5.8 and 2.2 x 10^{-6} $°C^{-1}$.

The composites sintered by the SPS technique had the highest densities and consequently had better mechanical properties, obtaining values between 5 and 9 GPa, Young's modulus between 78 and 105 GPa, always being the highest values

for the composite LZS+5A. The thermal conductivity ranged from 3 to 3.35 $W \cdot m^{-1}K^{-1}$ and the CTE also varied within a relatively large range, i.e. between 11.8 and 4.7 x 10^{-6} $°C^{-1}$.

Acknowledgments

This work has been supported by Ministerio de Economía y Competitividad (MINECO) and FEDER Funds under grant Nº MAT2016-67586-C3-R. Authors greatly acknowledge the financial Support of CAPES in the frame of the International Cooperation Program Science without Borders for Special Visiting Researcher PVE (MEC/MCTI/CAPES/CNPq/FAPs/N°71/2013), Project no. A011/2013. A. Borrell acknowledges the MINECO for her *Juan de la Cierva-Incorporación* contract (IJCI-2014-19839).

REFERENCES

[1] X. Song, Z. Sun, Q. Huang, M. Rettenmayr, X. Liu, M. Seyring, G. Li, G. Rao, F. Yin, Adjustable Zero Thermal Expansion in Antiperovskite Manganese Nitride, Advanced Materials 23(40) (2011) 4690-4694.

[2] M.F. Zawrah, E.M.A. Hamzawy, Effect of cristobalite formation on sinterability, microstructure and properties of glass/ceramic composites, Ceramics International 28(2) (2002) 123-130.

[3] A. Sommers, Q. Wang, X. Han, C. T'Joen, Y. Park, A. Jacobi, Ceramics and ceramic matrix composites for heat exchangers in advanced thermal systems—A review, Applied Thermal Engineering 30(11–12) (2010) 1277-1291.

[4] D. Jakobsen, W. Zhang, N. Doynov, A. Böhm, J. Malzbender, V. Michailov, A. Roosen, Thermal shock behaviour of laminated multilayer refractories for steel casting applications reinforced by residual stresses, Ceramics International 42(12) (2016) 13562-13571.

[5] R.M.D. Nascimento, A.E. Martinelli, A.J.A. Buschinelli, Review Article: recent advances in metal-ceramic brazing, Cerâmica 49 (2003) 178-198.

[6] F. Ribeiro, J. Maçaira, R. Cruz, J. Gabriel, L. Andrade, A. Mendes, Laser assisted glass frit sealing of dye-sensitized solar cells, Solar Energy Materials and Solar Cells 96 (2012) 43-49.

[7] Y. Fang, T.J. Hyde, F. Arya, N. Hewitt, P.C. Eames, B. Norton, S. Miller, Indium alloy-sealed vacuum glazing development and context, Renewable and Sustainable Energy Reviews 37 (2014) 480-501.
[8] K.-L. Lin, M. Singh, R. Asthana, Characterization of yttria-stabilized-zirconia/stainless steel joint interfaces with gold-based interlayers for solid oxide fuel cell applications, Journal of the European Ceramic Society 34(2) (2014) 355-372.
[9] K.S. Weil, The state-of-the-art in sealing technology for solid oxide fuel cells, JOM 58(8) (2006) 37-44.
[10] I.J. Induja, K.P. Surendran, M.R. Varma, M.T. Sebastian, Low κ, low loss alumina-glass composite with low CTE for LTCC microelectronic applications, Ceramics International 43(1, Part A) (2017) 736-740.
[11] J.D.T.M.A.P.L.B.C.S.V.C.A.P.N.d. Oliveira, PHYSICAL-MECHANICAL BEHAVIOUR OF A LZS GLASS-CERAMIC, Materials Science Forum 775-776 (2014) 5.
[12] J.D.O. Teixeira, Antonio Pedro Novaes; Bohels, Lourival; Cesconeto, Franciely Roussenq; Siligardi, Cristina; Pereira, Manuel Antonio., SIntering Behaviour of LZS glass-ceramics, Materials Science Forum 727-728 (2012) 7.
[13] A. de Oliveira, C. Leonelli, T. Manfredini, G. Pellacani, G. Ramis, M. Trombetta, Properties of glasses belonging to the Li2O–ZrO2–SiO2 system, Physics and chemistry of Glasses 39(4) (1998) 213-221.
[14] O.R.K. Montedo, F.M. Bertan, R. Piccoli, D. Hotza, A.N. Klein, A.P.N. de Oliveira, Low Thermal Expansion Sintered LZSA Glass-Ceramics. (Cover story), American Ceramic Society Bulletin 87(7) (2008) 34-40.
[15] O.R.K. Montedo, F.J. Floriano, J.d.O. Filho, Sintering kinetics of a 18.8Li2O 8.3ZrO2 64.2SiO2 8.7Al2O3 glass ceramic, Ceramics International 37(6) (2011) 1865-1871.
[16] S. Arcaro, F.R. Cesconeto, F. Raupp-Pereira, A.P. Novaes de Oliveira, Synthesis and characterization of LZS/α-Al2O3 glass-ceramic composites for applications in the LTCC technology, Ceramics International 40(4) (2014) 5269-5274.
[17] S. Arcaro, M. Isabel Nieto, J.B. Rodrigues Neto, A.P. Novaes de Oliveira, R. Moreno, Al2O3 Nanoparticulate LZS Glass–Ceramic Matrix Composites for Production of Multilayered Materials, Journal of the American Ceramic Society (2016) n/a-n/a.

[18] S. Arcaro, M.I. Nieto, R. Moreno, A.P.N. de Oliveira, The influence of nano alumina additions on the coefficient of thermal expansion of a LZS glass–ceramic composition, Ceramics International 42(7) (2016) 8620-8626.
[19] A.P.N.d.O.T. Manfredini, Al2O3 Particulate-Reinforced LZS Glass Ceramic Matrix Composite in: T. Group (Ed.) 9th CIMTEC Word Ceram-ics Congress, Ceramics: Getting into the 2000's, Faenza, 1998, p. 8.
[20] M.T. Oliveira APN, Leonelli C, Pellacani GC, Physical properties of quenched glasses in the Li2O-ZrO2-SiO2 system, Journal of the American Ceramic Society 79 (1996) 2.
[21] S. Kemethmuller, A. Roosen, F. Goetz-Neunhoeffer, J. Neubauer, Quantitative analysis of crystalline and amorphous phases in glass-ceramic composites like LTCC by the rietveld method, Journal of the American Ceramic Society 89(8) (2006) 2632-2637.
[22] M. Sakata, M.J. Cooper, Analysis of the Rietveld Profile Refinement Method, J Appl Crystallogr 12(Dec) (1979) 554-563.
[23] H.M. Rietveld, The Rietveld method, Phys Scripta 89(9) (2014).
[24] O. Burgos-Montes, R. Moreno, M.T. Colomer, J.C. Farinas, Synthesis of mullite powders through a suspension combustion process, Journal of the American Ceramic Society 89(2) (2006) 484-489.
[25] R. Moreno, J. Moya, J. Requena, Electroquímica de suspensiones cerámicas, Bol. Soc. Esp. Ceram. Vidr 26(6) (1987) 355-365.
[26] W. Höland, E. Apel, C. van't Hoen, V. Rheinberger, Studies of crystal phase formations in high-strength lithium disilicate glass–ceramics, Journal of non-crystalline solids 352(38) (2006) 4041-4050.
[27] G.B. W. Holand, Glass-Ceramic Technology, The American Ceramic Society, Westerville, 2002.
[28] B.D. Cullity, Elements of X-ray Diffraction, (2001).
[29] T. Bhosale, A. Gaikwad, Preparation and Characterization of Lithium Zirconium Silicate for CO2 Capture, Bulletin of Chemical Reaction Engineering & Catalysis 9(3) (2014) 249-262.
[30] H. Pfeiffer, P. Bosch, S. Bulbulian, Sol–gel synthesis of Li2ZrSi6O15 powders, Journal of Materials Chemistry 10(5) (2000) 1255-1258.
[31] P. Quintana, R. West, Synthesis of Li 2 ZrSi 6 O 15, a Zektzerite-Related Phase, Mineral. Mag 44(9) (1981) 361-362.

[32] R.M. German, Sintering theory and practice, Solar-Terrestrial Physics (Solnechno-zemnaya fizika) (1996) 568.